Preparation and Characterization of LaCr0.99Fe0.01O3 Nanomaterial

Preparation and Characterization of $LaCr_{0.99}Fe_{0.01}O_3$ Nanomaterial

M Erianti [1], **R Situmeang**[2], **S Sembiring**[3]

[1] Graduate School of Chemistry Department, University of Lampung, Jl. Sumantri Brojonegoro no 1, Bandar Lampung, Indonesia
[2] Department of Chemistry, Faculty of Mathematics and Natural Sciences, University of Lampung, Jl. Sumantri Brojonegoro no 1, Bandar Lampung, Indonesia
[3] Department of Physics, Faculty of Mathematics and Natural Sciences, University of Lampung, Jl. Sumantri Brojonegoro no 1, Bandar Lampung, Indonesia

email: mahlianie12@gmail.com[1], rudy.tahan@fmipa.unila.ac.id[2]

Abstract. Perovskite compounds show great potential in a variety of applications due to their diverse and unique properties and can be modified. Nanomaterial $LaCr_{0.99}Fe_{0.01}O_3$ has been prepared using sol-gel and freeze drying methods. The nanomaterial was then calcined at 700ºC for 10 hours and characterized by the analysis techniques of X-Ray Diffraction (XRD), Fourier Transform Infrared (FTIR), Diffuse Reflectance UV-Vis Spectroscopy (DRS UV-Vis), and Transmission Electron Microscopy (TEM). The result of XRD analysis showed that two main crystal phases were formed from the ABO_3 perovskite structure, namely $LaCrO_3$ and $LaFeO_3$ which were superimposed and the crystalline phase size based on the Scherrer method was 23.5 nm. Furthermore, the TEM analysis result shows that there are various forms and hollows. Then, the FTIR spectrum states that there is an interaction between transition metals, and the band gap energy is 2.71 eV.

Keywords: perovskite, nanomaterial, hollow, bandgap energy

1. Introduction

Perovskite material is well known as a material with many benefits [1–4], and each year researchers publish more than 2000 articles in various applications [5] related to perovskite material. The uniqueness of perovskite compounds, especially the type of oxide, is due to the ease of controlling the valence of the cations at A and B sites through partial substitution as well as non-stoichiometry control through cationic or anionic vacancies in their oxide structure based on an electroneutralite point of view [6]. This control leads to the existence of various cationic oxidation states which have characteristics as catalysts [7-9], ferroelectricity [10, 11], piezzoelectricity [12, 13], pyroelectricity [14, 15], thermolectricity [16], magnetism [17, 18], superconductivity [19, 20], sensors [21-23], optics [24, 25], and fuel cells [26] so that the application of oxide-type perovskite materials has proven to be very wide [27].

Oxide-type perovskites can be prepared from transition metal oxides or their salts using a variety of preparation methods such as hydrothermal [28-30], co-precipitation [31-33], and sol-gel [34, 35]. In general, the perovskite structure is ABO_3 although the cations at sites A and B can be modified such as $A_1A_2BO_3$ or $AB_1B_2O_3$. It can even be more complex $A_1A_2B_1B_2O_3$ and the structural model can be presented in Figure 1 below.

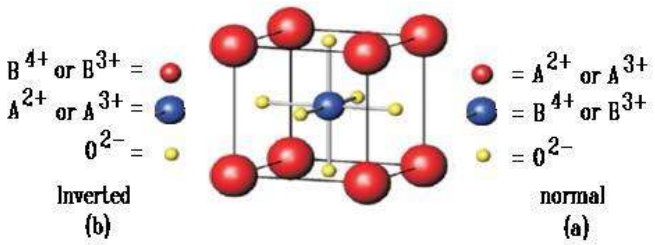

Figure 1. (a) normal dan (b) inverted Perovkite Structure

The success of preparing perovskite compounds depends also on the selection of cations for sites A and B, which generally follow the following rules,

$$t = \frac{(r_A + r_O)}{\sqrt{2}(r_B + r_O)}$$

Where t is the Goldschmidt tolerance factor, r_A, r_B, and r_O are the radii of A, B, and oxygen ions, respectively. The value of the Goldschmidt tolerance factor must be in the range from 0.75 to 1.00 in order to obtain the perovskite structure [36]. Several combinations of A- and B-site cations can form a stable perovskite-like structure. Additionally, A- and B-site cations, as well as oxygen anions can be partially substituted by other suitable elements [37, 38].

Based on the unique characteristics and flexibility of its structure [39, 40], where the A cation and the B cation that fill the octahedral and tetrahedral positions can exchange even be replaced by other inorganic cations or organic molecules. So that the modified perovskite material provides the desired characteristics for its application [41, 42]. One of the most commonly known perovskite oxide types is lanthanum chromite, $LaCrO_3$ with a wide range of applications such as electronics, opto-electronics, energy storage, thermal catalysis, sensors and photocatalysts [43-46].

In the field of photocatalysis, one of the characteristics of the $LaCrO_3$ perovskite as a reference is the ease of promoting electrons from the valence band (HOMO) to the conductance band (LUMO). The smaller the energy required to move electrons from the valence band to the conductance band, the greater the chance that the electrons will initiate the target reaction. Based on the obtained references, the perovskite gap energy of $LaCrO_3$ and its modification is in the ≤ 3.0 eV range [47, 48] so that the perovskite of this type of oxide can function as a photocatalyst because it is semiconductor [49].

On this occasion, we reported the preparation and characteristics of perovskite oxide types of lanthanum chromites doped with Fe cation, $LaCr_{0.99}Fe_{0.01}O_3$ using the sol gel method and its possible application in photocatalytic reaction by analyzing the material using X-Ray Diffraction, Fourier Transform Infrared, Diffuse Reflectance UV-Vis Spectroscopy, and Transmission Electron Microscopy.

2. Experimental

2.1. Material

The materials used in this study include $La(NO_3)_2$. 6 H_2O (Merck, 99%), $Cr(NO_3)_2$. 9 H_2O (Merck, 99%), $Fe(NO_3)_2$. 9 H_2O (Merck, 99%), NH_3 (Merck, 99%), pectin and distilled water.

2.2. Instruments

The instruments used for characterization include X-Ray Diffractometer (XRD) model PW 1710 with Cu-Kα radiation for structure identification, Fourier Transform Infrared (FTIR) type Shimadzu Prestige-21 for functional group identification, Diffuse Reflectance UV-Vis Spectroscopy (Agilent Cary 60) to determine the band-gap energy, and Transmission Electron Microscopy (TEM) JEOL JEM 1400 for identifying grain size distribution and crystallite morphology.

2.3. Preparation of $LaCr_{0.99}Fe_{0.01}O_3$

The $LaCr_{0.99}Fe_{0.01}O_3$ nanocatalyst was prepared by the sol-gel method. The procedure was described in the previous work [50].

2.4. Characterization of $LaCr_{0.99}Fe_{0.01}O_3$

2.4.1. X-Ray Diffraction Analysis. The X-ray diffraction pattern $LaCr_{0.99}Fe_{0.01}O_3$ was recorded at 2θ = 10-90º using a Philips diffractometer model PW 1710 Cu-Kα radiation. Phase identification was carried out by matching the diffractogram of the sample to the standard diffractogram using the JCPDF published by ICCD PDF. The particle size was determined by the Scherrer method [51].

2.4.2. FTIR Analysis. After heating at 90ºC, the samples were analyzed using FTIR spectroscopy. Spectroscopic analysis is performed by grinding the sample with KBr and scanning it at a wave number 4000-400 cm^{-1} [52].

2.4.3. UV-Vis DR Spectroscopy Analysis. Determination of the $LaCr_{0.99}Fe_{0.01}O_3$ band-gap energy, a number of samples were analyzed using UV-Vis Diffuse Reflectance Spectroscopy and scanned at a wavelength of 200-800 nm [53].

2.4.4. Transmission Electron Microscope Analysis. To evaluate the surface morphology, the samples were characterized using TEM. The analysis was conducted on polished and thermally etched samples with different magnifications [54].

3. Results and Discussion

3.1. Structural Analysis of X-Ray Diffractogram

Based on the diffractogram shown in Figure 2, the diffraction pattern of $LaCr_{0.99}Fe_{0.01}O_3$ was compared with the standard using the JCPDF program. The results showed that two main crystalline phases were formed which is superimpossed with each other, namely $LaCrO_3$ (PDF-24-1016) and $LaFeO_3$ (PDF-37-1493) with the highest intensity at 2θ = 32º. The crystal size of the sample is determined by the following Scherrer equation:

$$D = \frac{K\lambda}{\beta cos\theta}$$

Where K is the crystallite form factor, λ is the X-ray wavelength (1.5406 nm for CuKα), β is the width of the diffraction peaks, and θ is the Bragg angle. The average size of the crystalline phase of $LaCr_{0.99}Fe_{0.01}O_3$ was 23.5 nm.

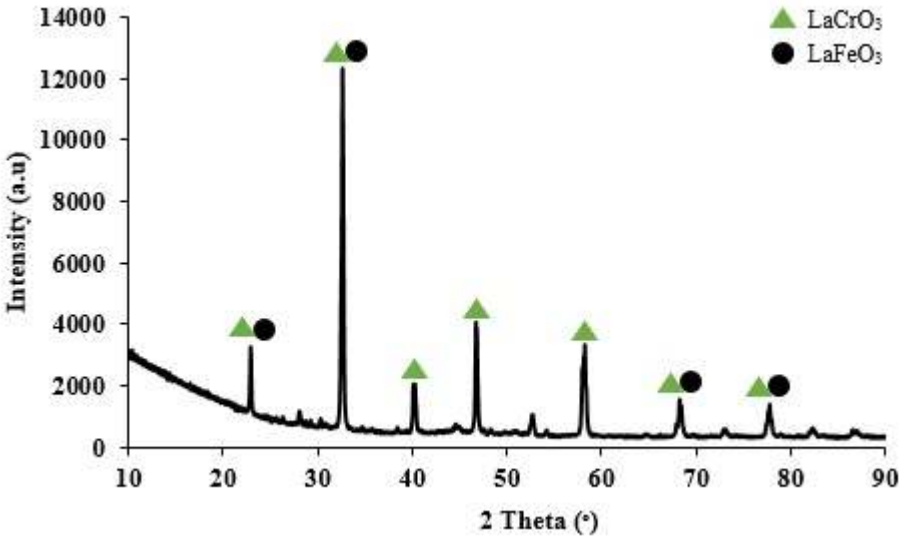

Figure 2. Diffractogram of $LaCr_{0.99}Fe_{0.01}O_3$ nanomaterial

3.2. Analysis of FTIR Spectrum

Figure 3 shows the FTIR spectra of the $LaCr_{0.99}Fe_{0.01}O_3$ nanomaterial prepared at a calcination temperature of 700ºC in the wave number range 4000-400 cm^{-1}. The FTIR spectrum of $LaCr_{0.99}Fe_{0.01}O_3$ is shown in Figure 4. The broad band observed at 3445 cm^{-1} and 1636 cm^{-1} corresponds to the stretching vibration and bending vibration of O-H groups respectively. The symmetric stretching of carboxyl C=O bond was not observed at 2356 cm^{-1} due to the adsorption of atmospheric carbon dioxide, as the measurement was recorded with pretreatment. The weaker intense

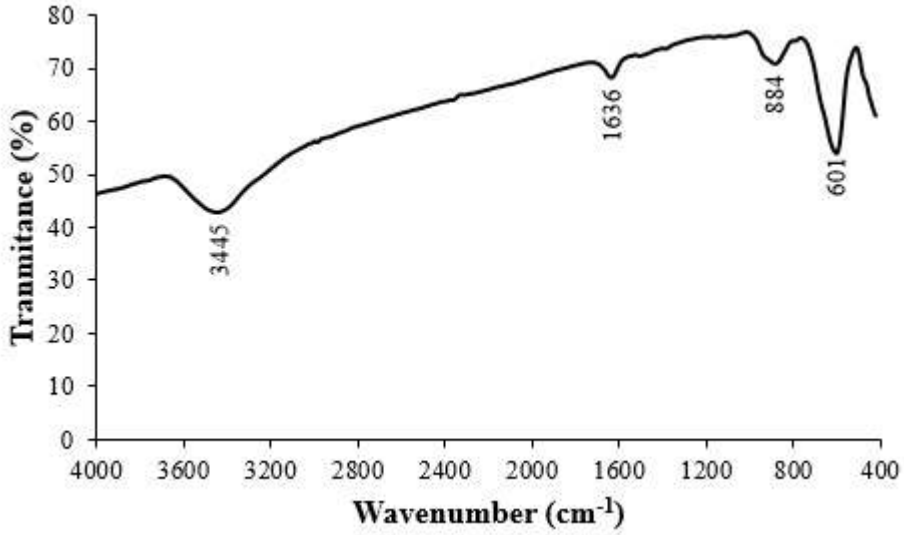

Figure 3. FTIR Spectrum of $LaCr_{0.99}Fe_{0.01}O_3$ nanomaterial

peak as a shoulder observed at around 500 cm^{-1} due to the presence of stretching vibration of Fe-O confirms the octahedral FeO_6 present in the $LaCr_{0.99}Fe_{0.01}O_3$ [55]. At the wave number 601 cm^{-1}, it shows the presence of Fe-O stretching vibrations [56] and La-O-La bending vibrations [57]. The presence of Cr-O and O-Cr-O stretching vibrations at 884 cm^{-1} absorption [58].

3.3. Analysis of DRS Spectrum

Optical absorption bands were detected on perovskite $LaCr_{0.99}Fe_{0.01}O_3$ through the % reflectance and absorbance spectra of the wavelength in Figure 4 above, where the four basins in Figure 4A at wavelengths of about 380, 450, 620, and 740 nm show absorption peaks in Figure 4B. The peaks indicate that there is an interaction between the 3d Fe^{3+} orbital and the 3d Cr^{3+} orbitals with the 2p O^{2-} orbitals, respectively, which are shown at the 380 and 450 nm wavelengths of absorption, respectively. Most probably week absorption bands at 630 and 740 nm belongs to d-d transition in Fe^{3+} and Cr^{3+} ion in an octahedral symmetry [58], which is influenced by replacing Cr with Fe in $LaCr_{0.99}Fe_{0.01}O_3$ perovskite structure. Intra-atomic d-d transitions are of much lower intensity comparison to the inter-atomic transitions at region of fundamental absorption edge, which are mainly determining the color of iron-rich oxides [59].

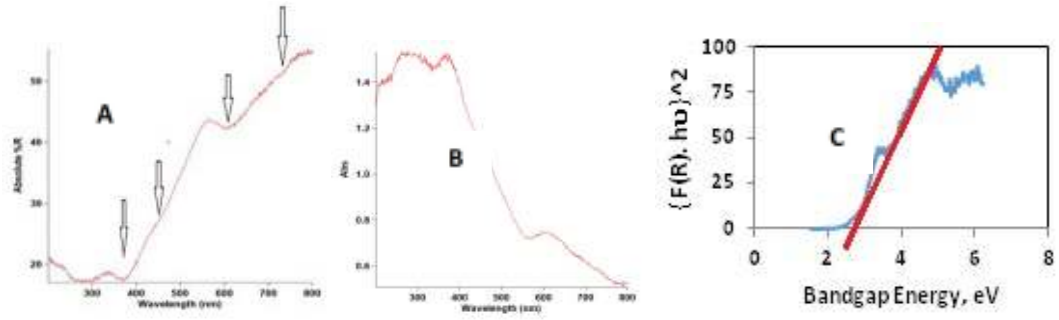

Figure 4. UV-Vis DR Spectra of $LaCr_{1-x}Fe_xO_3$

Figure 4C shows the bandgap energy obtained graphically through extrapolation when $\{F(R).h\nu\}^2 = 0$ to bandgap energy (E_g) on the X-axis of 2.71 eV. Order 2 in the equation $(F(R).h\nu)^2$ denotes an electronic transition that occurs indirectly. Based on the E_g value obtained, it can be said that the $LaCr_{0.99}Fe_{0.01}O_3$ nanomaterial can function as a photocatalyst.

3.4. Morphological Analysis

Characterization of the samples using TEM produced the micrographs as presented in Figure 5 below. In general, there are several structural shapes identified such as cubic (brown arrow), circular (yellow arrow) and pipe (blue arrow). If focusing on perovskite structure, it displays, the existence of $LaCr_{0.99}Fe_{0.01}O_3$ crystalline phase as a unit cell since $LaCrO_3$ and $LaFeO_3$ is superimpossed. However, in a certain area, the presence of a bigger perovskite structure can be observed, which confirms the existence of layers (red arrow) and hollow cubes (green arrow).

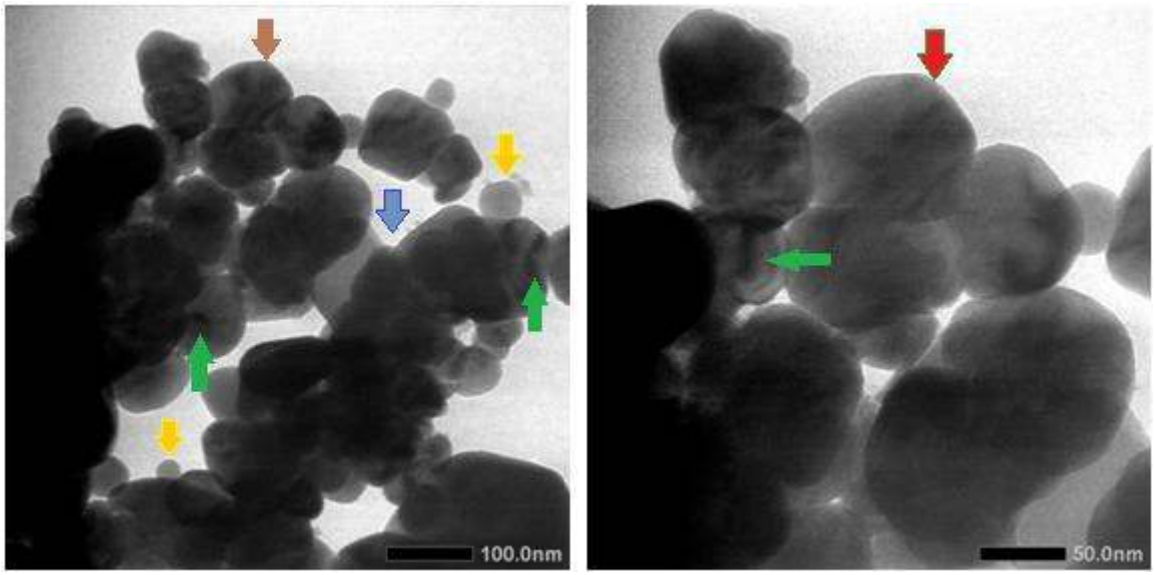

Figure 5. TEM Micrograph of $LaCr_{0.099}Fe_{0.01}O_3$

Although various forms of perovskite appear to exist, the resulting sizes are mostly in the nano category. It seems that further analysis is needed regarding the hallow form. Based on the 50 nm scale (right-micrograph), it can be said that the grains are 50-100 nm in size. Few grains appeared to be in the planar connection so that they seem to be greater than 100 nm, and a few appear as circular with a size less than 50 nm. In addition, there was a tube with a diameter of 98 nm and its length of 163.3 nm. Overall result proved that the material prepared is nano size and hollow. The size result is smaller than that of $LaCrO_3$ modified by Fe and Co which is 168 nm [60].

4. Conclusion

Based on the analysis of $LaCr_{0.99}Fe_{0.01}O_3$ material characteristics, it can be concluded that the prepared materials have the perovskite structure consisting of $LaFeO_3$ and $LaCrO_3$ which is superimposed and formed into layers or piles that stick together. In fact, the structure formed is various. It has nanopipes, nanocubes, nanocircular and hollow structures. So that the perovskites are nano hollow material. Furthermore, since its band-gap energy is around 3.0 eV, it is implied that this material could be used in photonic applications.

Acknowledgments

Our gratitude is announced to the Research Directorate and Social Services , Research Deputy and the Ministry of Research Development and Technology/National Research Institution and Innovation (BRIN) and the Research Institution of University of Lampung (LPPM) for research funding provided through the Competitive Research Grant, with research contract No. 289 / SP2H / LT / DRPM / 2020 and the Integrated Services Unit of Integrated Laboratory and the Technology Innovation Centre, the University of Lampung for analyzing the samples.

References

[1] Theofylaktos L, Kosmatos K O, Giannakaki E, Kourti H, Deligiannis D, Konstantakou M and Stergiopoulos T 2019 Perovskites with d-block metals for solar energy applications *Dalton Trans.* **48**(26) 9516-9537

[2] King G and Woodward P M 2010 Cation ordering in perovskites *J. Mat. Chem*. **20**(28) 5785–5796

[3] Assirey E A R 2019 Perovskite synthesis, properties and their related biochemical and industrial application *Saudi Pharm. J.* **27**(6) 817–829
[4] Sangiorgi N, Aversa L, Tatti R, Verucchi R and Sanson A 2017 Spectrophotometric method for optical band gap and electronic transitions determination of semiconductor materials. *Opt. Mater.* **64** 18–25
[5] Royer S and Duprez D 2011 Catalytic oxidation of carbon monoxide over transition metal oxides *ChemCatChem*. **3**(1) 24–65
[6] Andreasson J, Holmlund J, Knee C S, Käll M, Börjesson L, Naler S, Bäckström J, Rübhausen M, Azad A K and Eriksson Sten-G 2007 Franck-Condon higher order lattice excitations in the $LaFe_{1-x}Cr_xO_3$ (x=0, 0.1, 0.5, 0.9, 1.0) perovskites due to Fe-Cr charge transfer effects *Phys. Rev. B* **75**(10) 104302
[7] Foo G S, Polo-Garzon F, Fung V, Jiang D E, Overbury S H and Wu Z 2017 Acid–base reactivity of perovskite catalysts probed via conversion of 2-propanol over titanates and zirconates *ACS Catal.* **7**(7) 4423–4434
[8] Situmeang R, Supriyanto R, Septanto M, Simanjuntak W, Sembiring S and Roger A C 2013 $Ni_xCo_yFe_{1-x-y}O_4$ nanocatalyst: preparation, characterization, and acitvity in CO_2/H_2 conversion proc *The 2nd Int. Conf. Indones. Chem. Soc.* (October 22-23th Yogyakarta: Universitas Islam Indonesia) pp 103–110
[9] Chawla S K, George M, Patel F and Patel S 2013 Production of synthesis gas by carbon dioxide reforming of methane over nickel based and perovskite catalysts *Proc. Eng.* **51** 461–466
[10] Weidenkaff A, Ebbinghaus S G, Lippert T, Montenegro M J, Soltmann C and Wessicken R 2002 Phase formation and phase transition of $Ln_{1-x}Ca_xCoO_{3-\delta}$ (Ln = La, Er) applied for bifunctional air electrodes *Cryst. Eng.* **5**(3-4) 449–457
[11] Weidenkaff A 2004 Preparation and application of nanostructured perovskite phases *Adv. Eng. Mater.* **6**(9) 709–714
[12] Kim Yun-J, Dang Tran-V, Choi Hyung-J, Park Byeong-J, Eom Ji-H, Song Hyun-A, Seol D, Kim Y, Shin Sung-H, Nah J and Yoon Soon-G 2016 Piezoelectric properties of $CH_3NH_3PbI_3$ perovskite thin films and their applications in piezoelectric generators *J. Mater. Chem. A* **4**(3) 756–763
[13] Zheng T, Wu J, Xiao D and Zhu J 2018 Recent development in lead-free perovskite piezoelectric bulk materialsn *Prog. Mat. Sci.* **98** 552-624
[14] Li S, Zhao Z, Zhao J, Zhang Z, Li X and Zhang J 2020 Recent advances of ferro-, piezo-, and pyroelectric nanomaterials for catalytic applications *ACS Appl. Nano Mater.* **3**(2) 1063–1079
[15] Moalla R, Cueff S, Penuelas J, Vilquin B, Saint-Girons G, Baboux N and Bachelet R 2018 Large anisotropy of ferroelectric and pyroelectric properties in heteroepitaxial oxide layers *Scientific Reports* **8** 4332
[16] Weidenkaff A, Robert R, Aguirre M, Bocher L, Lippert T and Canulescu S 2008 Development of thermoelectric oxides for renewable energy conversion technologies *Renew. Energy* **33**(2) 342–347
[17] Raveau B 2007 The perovskite history: More than 60 years of research from the discovery of ferroelectricity to colossal magnetoresistance via high TC superconductivity *Prog. Solid State Chem.* **2**(35) 171–173
[18] Sun B, Liu Xiao-F, Li Xiang-Y, Cao Y, Yan Z, Fu L, Tang N, Wang Q, Shao X, Yang D and Zhang Hao-L 2020 Reversible thermochromism and strong ferromagnetism in two-dimensional hybrid perovskites *Angew.Chem. Int. Ed.* **59** 203–208

[19] Ma X, Firdous A, Zhang L, Wu S, Zhang J, Liu L, Wang Y, Geng J, Sun J, Li G, Liao F and Lin J 2019 Superconductivity in perovskite $Ba_{1-x}K_xBi_{0.30}Pb_{0.70}O_{3-\delta}$. *Chem. Select* **4**(11) 3135–3139

[20] Vaitheeswaran G, Kanchana V, Svane A, and Delin A 2007 Elastic properties of $MgCNi_3$—a superconducting perovskite *J. Phys.: Condens. Matter*. **19**(32) 326214 (6pp)

[21] Thuy N T, Minh D L, Giang H T and Toan N N 2014 Structural, electrical, and ethanol-sensing properties of $La_{1-x}Nd_xFeO_3$ nanoparticles *Adv. Mater. Sci. Eng.* 685715

[22] Bektas M, Hanft D, Schönauer-Kamin D, Stöcker T, Hagen G and Moos R 2014 Aerosol-deposited $BaFe_{0.7}Ta_{0.3}O_{3-\delta}$ for nitrogen monoxide and temperature-independent oxygen sensing *J. Sens. Sens. Syst.* **3**(2) 223–229

[23] Josephine B A, Jeseentharani V, Teresita V M, George M and Antony S A 2013 Humidity sensing properties and temperature conductivity studies of sol-gel derived novel nanomaterials of lanthanum strontium chromites *Sens. Trans.* **156**(9) 304

[24] Chen C W, Hsiao S Y, Chen C Y, Kang H W, Huang Z Y and Lin H W 2015 Optical properties of organometal halide perovskite thin films and general device structure design rules for perovskite single and tandem solar cells *J. Mater. Chem. A* **3**(17) 9152–9159

[25] Liu B, Soe C M M, Stoumpos C C, Nie W, Tsai H, Lim K, Mohite A D, Kanatzidis M G, Marks T J and Singer K D 2017 Optical properties and modeling of 2D perovskite solar cells *Solar RRL* **1**(8) 1700062

[26] Yang Y and You J 2017 Make perovskite solar cells stable *Nature* **544**(7649) 155–156

[27] Cao Shao-W, Zhu Ying-J, Cheng Guo-F and Huang Yue-H 2009 $ZnFe_2O_4$ nanoparticles: microwave-hydrothermal ionic liquid synthesis and photocatalytic property over phenol *J. Hazard. Mater.* **171**(1-3) 431–435

[28] Li J, Wu Q and Wu J 2015 *Synthesis of nanoparticles via solvothermal and hydrothermal methods* (Switzerland: Springer international publishing) Handbook of nanoparticles pp 1–28

[29] Rivas-Vázquez L P, Rendón-Angeles J C, Rodríguez-Galicia J L, Gutiérrez Chavarria C A, Zhu K J and Yanagisawa K 2006 Preparation of calcium doped $LaCrO_3$ fine powder by hydrothermal method and its sintering. *J. Euro. Ceram. Soc.* **26**(1–2) 81–88

[30] Kumar S, Teraoka Y, Joshi A G, Rayalu S and Labhsetwar N J 2011 Ag promoted $La_{0.8}Ba_{0.2}MnO_3$ type perovskite catalyst for N_2O decomposition in the presence of O_2, NO and H_2O. *J. Mol. Catal.* **348**(1–2) 42–54

[31] Junwu Z, Xiaojie S, Yanping W, Xin W, Xujie Y and Lude L. 2007 Solution-phase synthesis and characterization of perovskite $LaCoO_3$ nanocrystals via a co-precipitation route. *J. Rar. Ear.* **25**(5) 601–604

[32] Doggali P, Rayalu S, Teraoka Y and Labhsetwar N 2015 Effect of A-site substitution in perovskites: catalytic properties of $PrMnO_3$ and Ba/K/Ce substituted $PrMnO_3$ for CO and PM oxidation. *J. Envir. Chem. Engine.* **3**(1) 420–428

[33] Adole V A, Pawar T B, Koli P B and Jagdale B S 2019 Exploration of catalytic performance of nano-La_2O_3 as an efficient catalyst for dihydropyrimidinone/thione synthesis and gas sensing. *J. Nanost. Chem.* **9** 61–76

[34] Situmeang R, Manurung P, Sulistiyo S T, Hadi S, Simanjuntak W, Sembiring S 2015 Sol-gel method for preparation of nanosize $NiFe_{2-x}Co_xO_4$ using egg white *Asian. J. Chem.* **27**(3) 1138–1142

[35] Girish H N, Shao G Q and Basavalingu B 2016 Well- monocrystallized $LaCrO_3$ Particles from $LaCrO_4$ precursor by supercritical hydrothermal technique *Roy. Soci. Chem.* **6**(83) 79763–79767

[36] Goldschmidt V M 1926 Die gesetze der krystallochemie *Die Naturwissenschaften* **14**(21) 477–485

[37] Ebbinghaus S G, Abicht H P, Dronskowski R, Müller T, Reller A and Weidenkaff A 2009 Perovskite-related oxynitrides—Recent developments in synthesis, characterisation and investigations of physical properties *Progr. Solid State Chem.* **37** (2-3) 173–205

[38] Yoon S, Maegli A E, Karvonen L, Matam S K, Shkabko A, Riegg S, Großmann T, Ebbinghaus S G, Pokrant S and Weidenkaff A 2013 Bandgap tuning in $SrTi(N,O,F)_3$ by anionic-lattice variation *J. Solid State Chem.* **206** 226–232

[39] Yang D, Yang R, Priya S and Liu S 2019 Recent advances in flexible perovskite solar cell: Fabrications and applications *Angew. Chemie Int. Ed.* **58**(14) 4466–4483

[40] Nakanishi T, Masuda Y and Koumoto K 2004 Site-Selective deposition of magnetite particulate thin films on patterned self-assembled monolayers *Chem. Mater.* **16**(18) 3484–3488

[41] Taffa D H, Dillert R, Ulpe A C, Bauerfeind K C, Bredow T, Bahnemann D W and Wark M 2016 Photoelectrochemical and theoretical investigations of spinel type ferrites ($M_xFe_{3-x}O_4$) for water splitting: A mini-review *J. Photon. Energy* **7**(1) 012009

[42] Acik M and Darling S B 2016 Graphene in perovskite solar cells: Device design, characterization and implementation. *J. Mater. Chem. A* **4**(17) 6185–6235

[43] Park J W and Lee K T 2018 Enhancing performance of $La_{0.8}Sr_{0.2}MnO_3$ d-in filtrated $Er_{0.4}Bi_{1.6}O_3$ cathodes via controlling wettability and catalyst loading of the precursor solution for IT-SOFCs *J. Ind. Eng. Chem.* **60** 505–512

[44] Giang H T, Duy H T, Ngan P Q, Thai G H, and Toan N N 2013 Effect of 3d transition metals on gas sensing characteristics of perovskite oxides $LaFe_{1-x}Co_xO_3$ *Anal. Methods* **5**(16) 4252–4257

[45] Pereñíguez R, Caballero A and Ferri D 2017 Preferential oxidation of CO on a La-Co-Ru perovskite-type oxide catalyst *Catal. Commun.* **92** 75–79

[46] Saddique M B, Rashid M, Afzal A, Ramay S M, Aziz F and Mahmood A 2017 Ground state opto-electronic and thermoelectric response of cubic $XSnO_3$ (X = Ba, Sr) compounds *Curr. Appl. Phys.* **17**(8) 1079–1086

[47] Situmeang R, Sembiring S, Simanjuntak W, Sembiring Z and Yuwono S D 2019 Characteristics of $LaCrO_3$ nanomaterial : the effect of the calcination temperature *J. Chem. Technol. Metall.* **54**(4) 715–720

[48] Naseem S, Khan W, Saad A A, Shoeb M, Ahmed H, Husain S and Naqvi A H 2014 Variation in band gap of lanthanum chromate by transition metals doping $LaCr_{0.9}A_{0.1}O_3$ (A:Fe/Co/Ni) *AIP Conf. Proc.* **1591**(1) 259-261

[49] Situmeang R 2020 Pectins: Extraction, Purification, Characterization and Applications, Edited by Martin Masuelli *Chapter 5*: *Pectins as an emulsifying agent on the Preparation, Characterization, and Photocatalysis of nano-$LaCrO_3$* (London-UK: IntechOpen Publisher) ISSN 2632-0003

[50] Djayasinga R and Situmeang R 2015 Preparation and characterization of nanosize spinel $Ni_{0.9}Fe_2Cu_{0.1}O_4$ using pectin as binding agent *Proc. IConSSE FSM SWCU* BC48-55

[51] Cullity B D 1978 *Elements of X-ray Diffraction,* 2nd ed. (London: Addison-Wesley) p.102
[52] Ryczkowski J 2001 IR spectroscopy in catalysis *Catal. Today* **68**(4) 263-381
[53] Sangiorgi N, Aversa L, Tatti R, Verucchi R and Sanson A 2017 Spectrophotometric method for optical band gap and electronic transitions determination of semiconductor materials. *Opt. Mater*. **64** 18–25
[54] Sridhara Rao D V, Muraleedharan K, Humphreys C J, in A. Méndez-Vilas, Díaz J (Eds.) 2010 *Microscopy: Science, Technology, Applications and Education* (Spain: Formatex)
[55] Vijayaraghavan T, Sivasubramanian R, Hussain S and Ashok A 2017 A facile synthesis of $LaFeO_3$-Based perovskites and their application towards sensing of neurotransmitters *Chem. Select* **2**(20) 5570–5577
[56] Situmeang R, Romiyati R, Saputra A A and Sembiring S 2020 $Ni_{0.5}V_{0.5}Fe_2O_4$ Nanophotocatalyst: Preparation, characterization and its activity on remazol golden yellow degradation under sunlight irradiation *Key Eng. Matter.* **840** 71-78 Trans Tech Publications Ltd.
[57] Situmeang R, Supryanto R, Kahar L N A, Simanjuntak W and Sembiring S 2017 Characteristics of nano-size $LaCrO_3$ prepared through sol-gel route using pectin as emulsifying agent. *Orient. J. Chem.* **33**(4) 1705-1713
[58] Situmeang R, Tamba M, Simarmata E, Yuliarni T, Simanjuntak W, Sembiring Z and Sembiring S 2019 $LaCrO_3$ nano photocatalyst: the effect of calcination temperature on its cellulose conversion activity under UV-ray irradiation *Adv. Nat. Sci.: Nanosci. and Nanotechnol.* **10**(1) 015009
[59] Virden A E and O'Grady K 2006 The temperature dependence of magnetization in ferofluids *J. Appl. Phys*. **99**(8) 08S106
[60] Rativa-Prada W, Gomez-Cuaspud J A, Vera-Lopez E, and Carda J B 2017 Structural and electrical study of $LaCrO_3$ modified with Fe and Co. J. Phys. Conf. Series 786 012029